Appendix A: Velocity moments and uncertainties

The lower and upper 1σ uncertainties on the estimations of the median velocities are calculated as

$$\sigma^{\rm low}_{\tilde{V}_i} = \sqrt{\frac{\pi}{2N}}(\tilde{V}_i - Per(V_i, 15.85)) \quad (A.1)$$

$$\sigma^{\rm upp}_{\tilde{V}_i} = \sqrt{\frac{\pi}{2N}}(Per(V_i, 84.15) - \tilde{V}_i), \quad (A.2)$$

respectively, where N is the number of stars in the cell, V_i is one of the three Galactocentric components of the velocity vector V_R, V_ϕ, or V_Z, and $\tilde{V}_i$ is the median of the distribution of V_i, and $Per(V_i, 15.85)$ and $Per(V_i, 84.15)$ are the 15.85th and 84.15th percentiles of the distribution of V_i, respectively.

The dispersions of the velocities are calculated as

$$\sigma_{V_i} = \frac{\mathrm{Per}(V_i, 84.15) - \mathrm{Per}(V_i, 15.85)}{2}, \quad (A.3)$$

using the same notation as above.

The lower and upper 1σ uncertainties on the estimation of the velocity dispersions are calculated as

$$\sigma^{\rm low}_{\sigma_{V_i}} = \frac{\sqrt{2\pi}}{e^{-0.5}}\sqrt{\frac{0.1585 \times 0.683}{N}}(\tilde{V}_i - Per(V_i, 15.85)) \quad (A.4)$$

$$\sigma^{\rm upp}_{\sigma_{V_i}} = \frac{\sqrt{2\pi}}{e^{-0.5}}\sqrt{\frac{0.1585 \times 0.683}{N}}(Per(V_i, 84.15) - \tilde{V}_i), \quad (A.5)$$

respectively, using the same notations as in Eqs. A.1 and A.2.

Appendix B: Biases induced by selections on the velocity uncertainties

Figures B.1 and B.2 show the median cylindrical velocities in the face-on view of the disc plane for the main sample and for an additional selection of stars with velocity errors in each component smaller than 2 km s^{-1}, respectively. It is evident from the comparison of all panels in the two figures that this cut in velocity error introduces strong biases in the median velocity field. The differences in median velocity can be of up to 20 km s^{-1}, and the global appearance of the velocity field changes substantially. The biases result from the correlations between velocities and velocity uncertainties. Selecting on the velocity uncertainties modifies the shape of the velocity distributions and therefore biases the measures of the moments of these distributions.

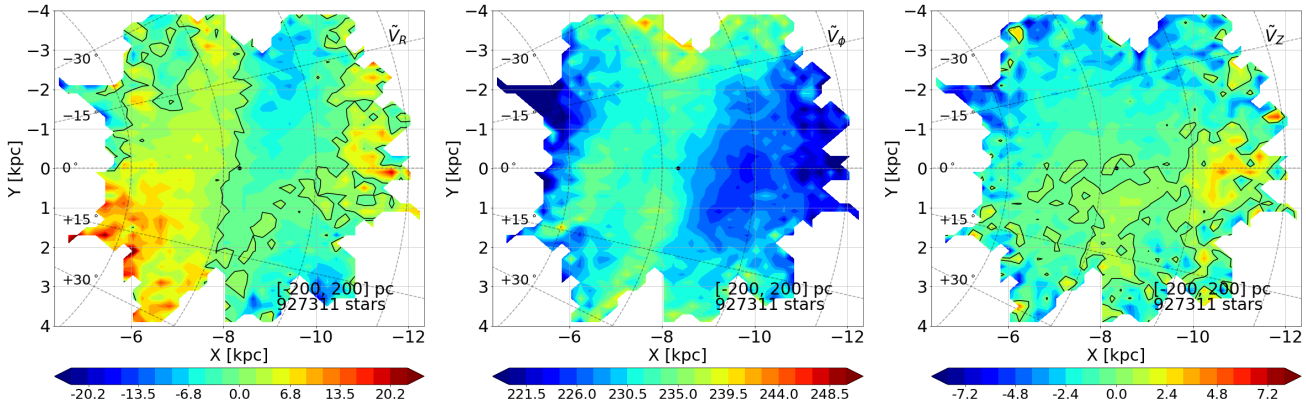

Fig. B.1. Face-on view of the kinematic of the disc mid-plane ([−200, +200] pc): Median radial velocity (*left*), median azimuthal velocity (*centre*), and median vertical velocity (*right*).

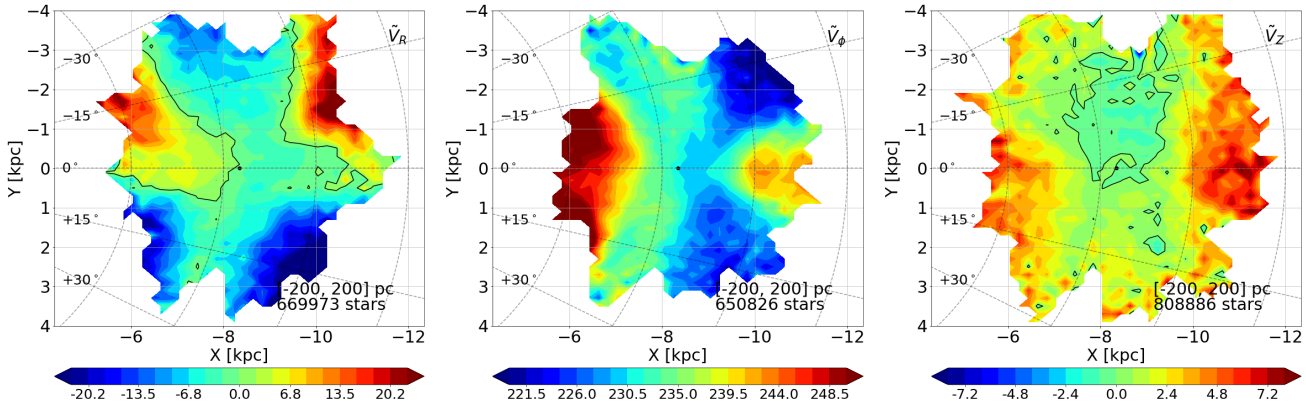

Fig. B.2. Same as Fig. B.1, but selecting the stars with uncertainties smaller than or equal to 2 km s^{-1} on the relevant component: $\sigma_{V_R} \leq 2$km s^{-1} (*left*), $\sigma_{V_\phi} \leq 2$km s^{-1} (*centre*), and $\sigma_{V_Z} \leq 2$km s^{-1} (*right*).

Appendix C: Velocity maps

This appendix contains the mosaics of face-on and edge-on maps of the median velocities: $\tilde{V}_R$ (Fig. C.1 and C.2), $\tilde{V}_\phi$ (Fig. C.3 and C.4), and $\tilde{V}_Z$ (Fig. C.5 and C.7), and of the velocity dispersions: σ_{V_R} (Fig. C.8 and C.9), σ_{V_ϕ} (Fig. C.10 and C.11), and σ_{V_Z} (Fig. C.12 and C.13).

The face-on map mosaics are made of nine maps, each one corresponding to a 400 pc height Z layer. The exception is the median vertical velocity, $\tilde{V}_Z$, whose mosaic is made of six maps: three above the disc mid-plane, and three below it. The edge-on map mosaics are made of four maps, each one corresponding to a 15 degrees slice in azimuth: $[-30, -15]$, $[-15, 0]$, $[0, +15]$ and $[+15, +30]$ degrees.

Figure C.6 shows the face-on maps of the bending and breathing velocities (defined in Sect. 3.1).

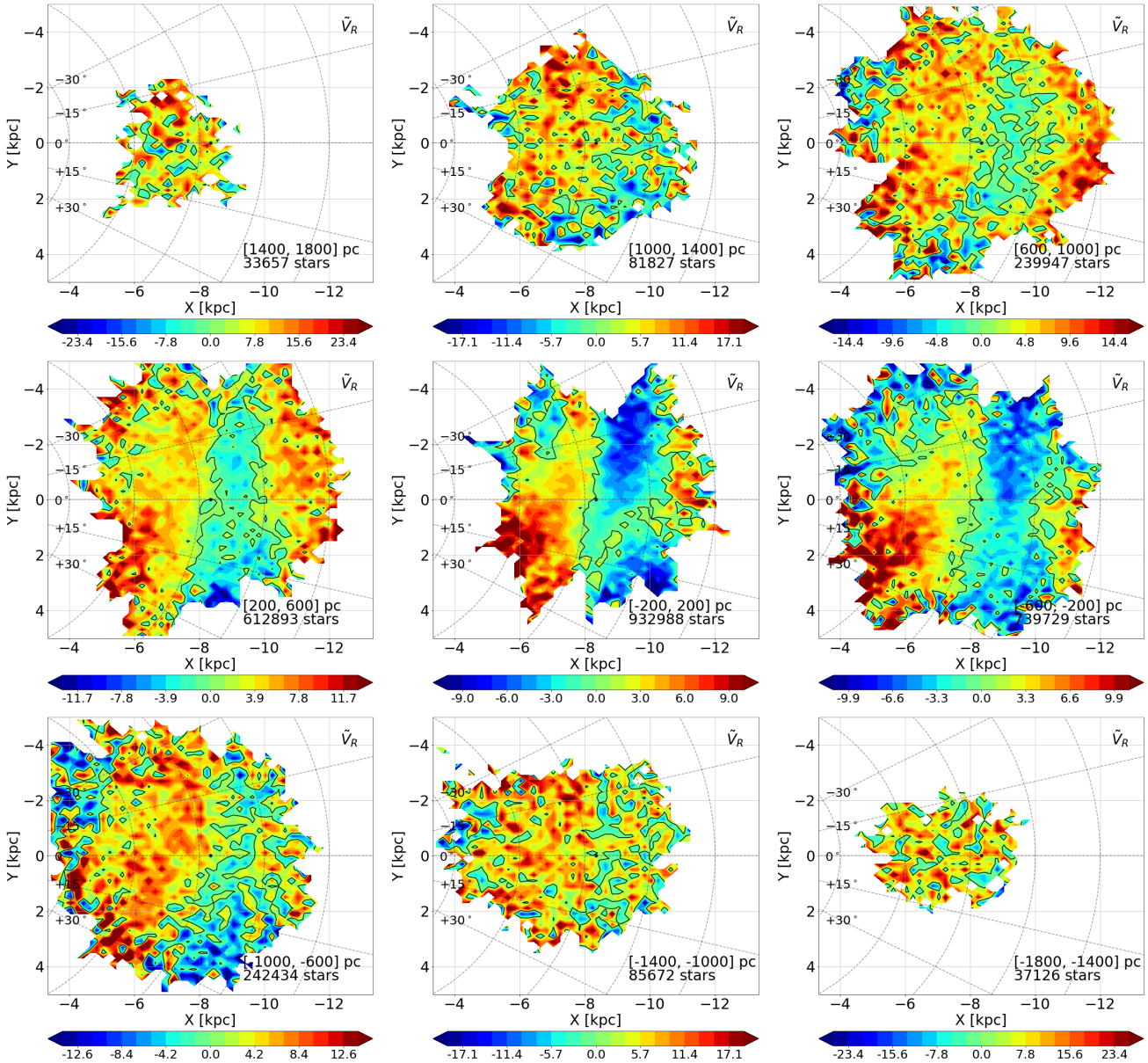

Fig. C.1. Mosaic of face-on maps of the median radial velocity, $\tilde{V}_R$, of the giant sample. Each map corresponds to a Z layer of 400 pc height, from $[+1400, +1800]$ pc (*top left*) to $[-1800, -1400]$ pc (*bottom right*). In each map, the azimuths increase clockwise. They are labelled from -30 to $+30$ degrees on the left of the maps. The Sun is represented by a black dot at $X = -8.34$ kpc and $Y = 0$ kpc. The Galactic centre is located on the left side. The Milky Way rotates clockwise. The iso-velocity contours $\tilde{V}_R = 0$ km s^{-1} are pointed out as black lines. The numbers of stars used to produce the maps are given in the lower left corners.

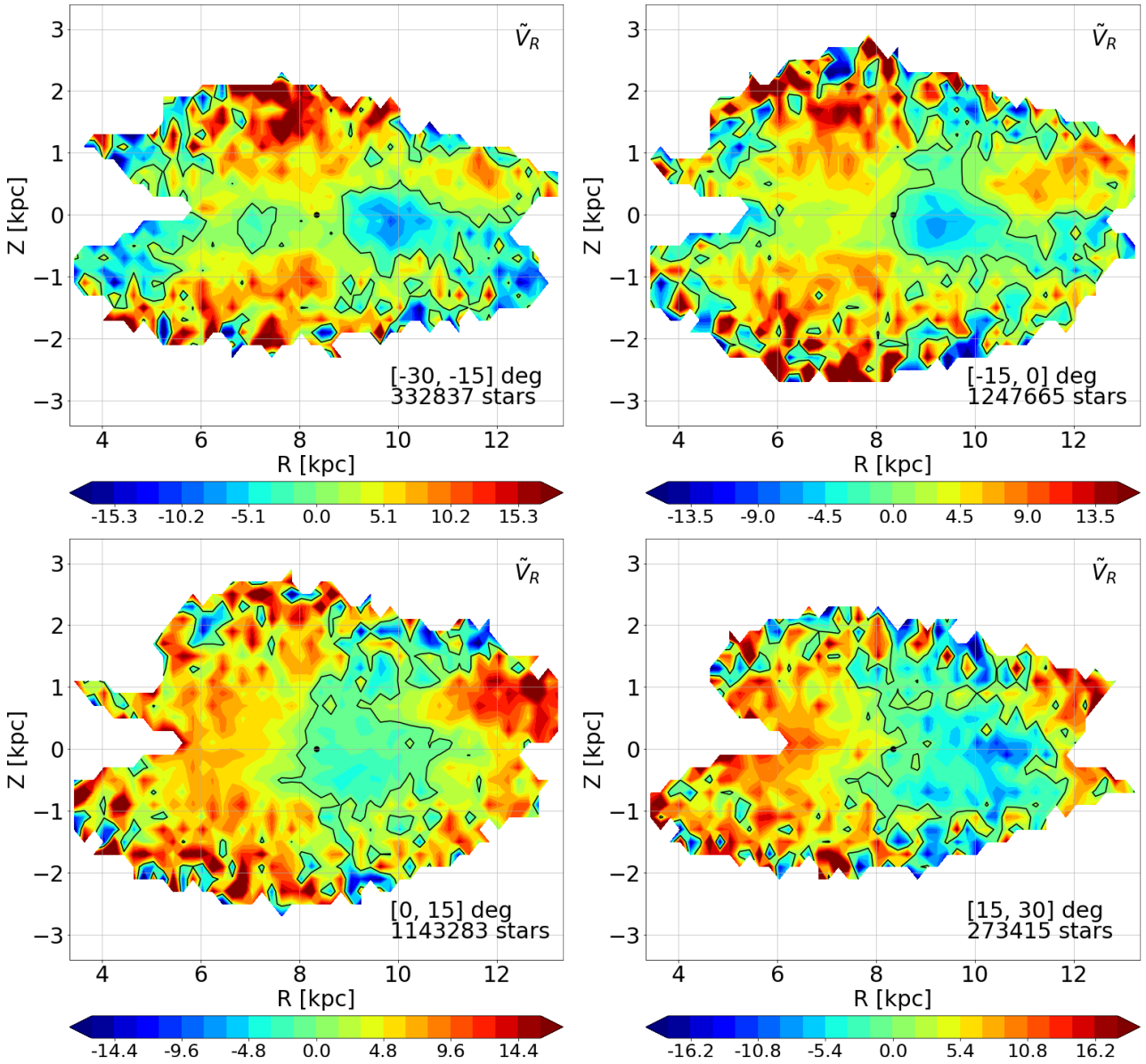

Fig. C.2. Mosaic of edge-on maps of the median radial velocity, $\tilde{V}_R$, of the giant sample. Each map corresponds to a slice of 15 degrees in azimuth: $[-30, -15]$ (*top left*), $[-15, 0]$ (*top right*), $[0, +15]$ (*bottom left*), and $[+15, +30]$ degrees (*bottom right*). The Sun is represented by a black dot at $X = -8.34$ kpc and $Y = 0$ kpc. The Galactic centre is located on the left side. The iso-velocity contours $\tilde{V}_R = 0$ km s^{-1} are pointed out as black lines. The numbers of stars used to produce the maps are given in the lower left corners.

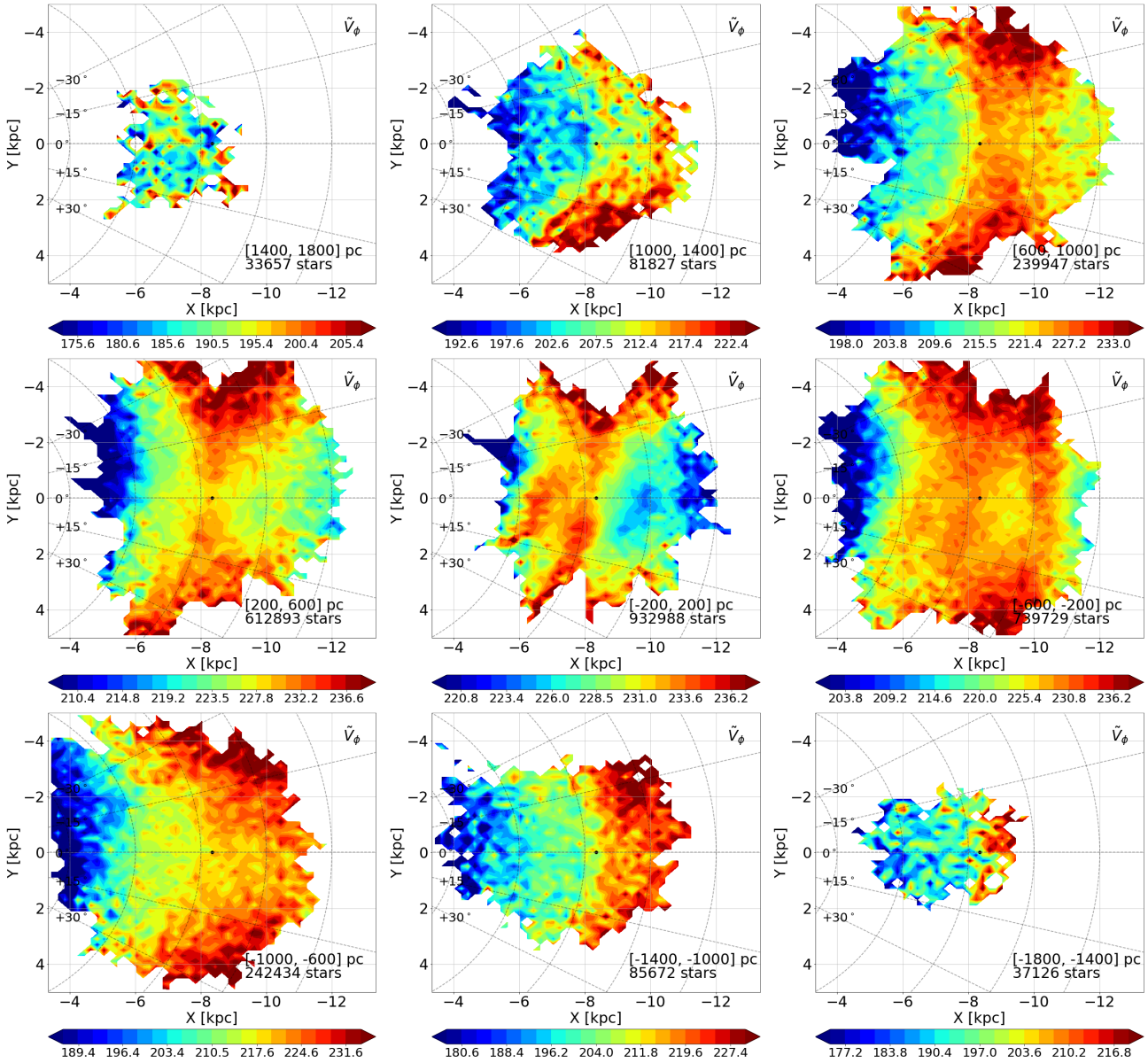

Fig. C.3. Same as Fig. C.1 for the median azimuthal velocity, $\tilde{V}_\phi$.

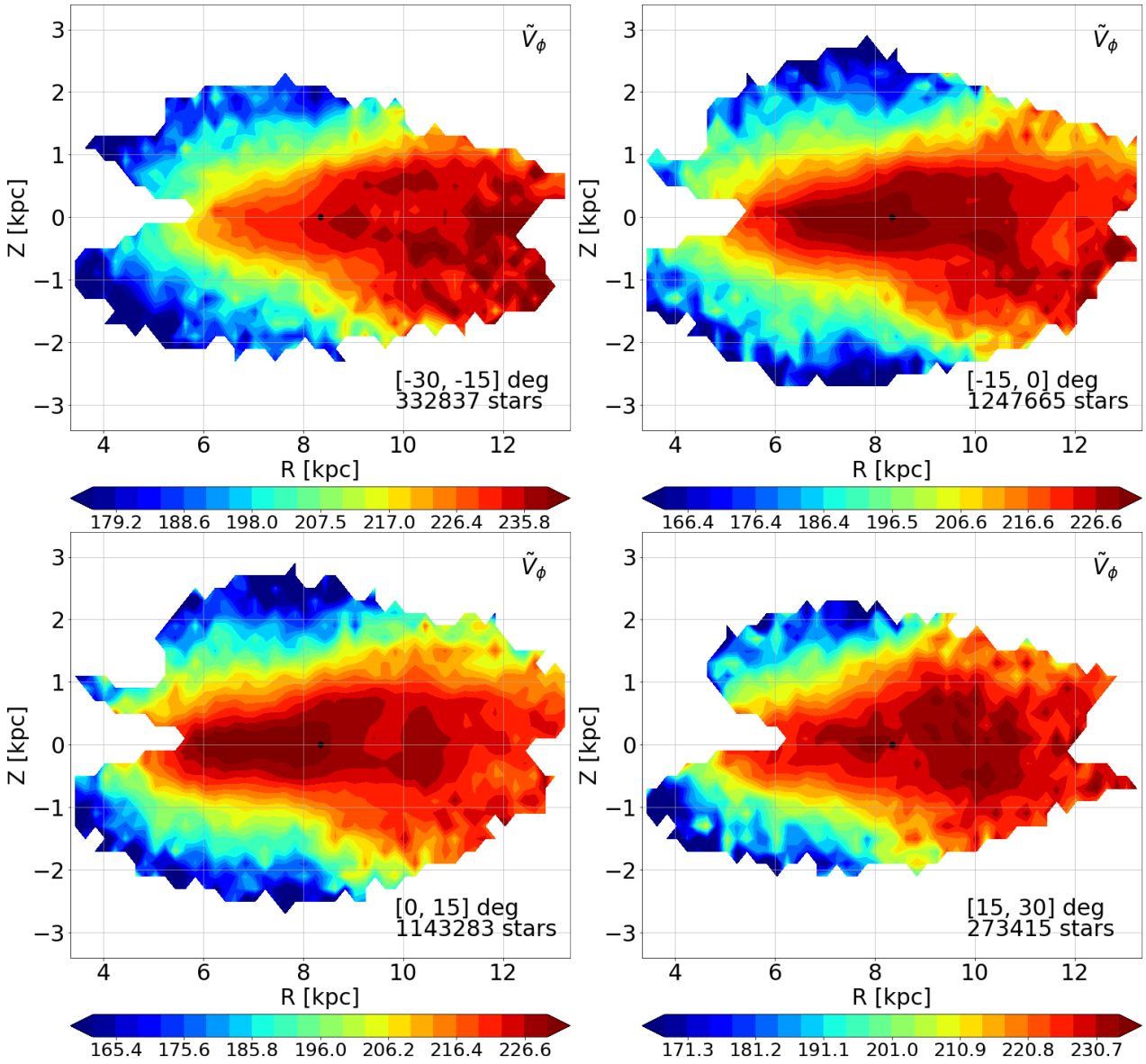

Fig. C.4. Same as Fig. C.2 for the median azimuthal velocity, $\tilde{V}_\phi$.

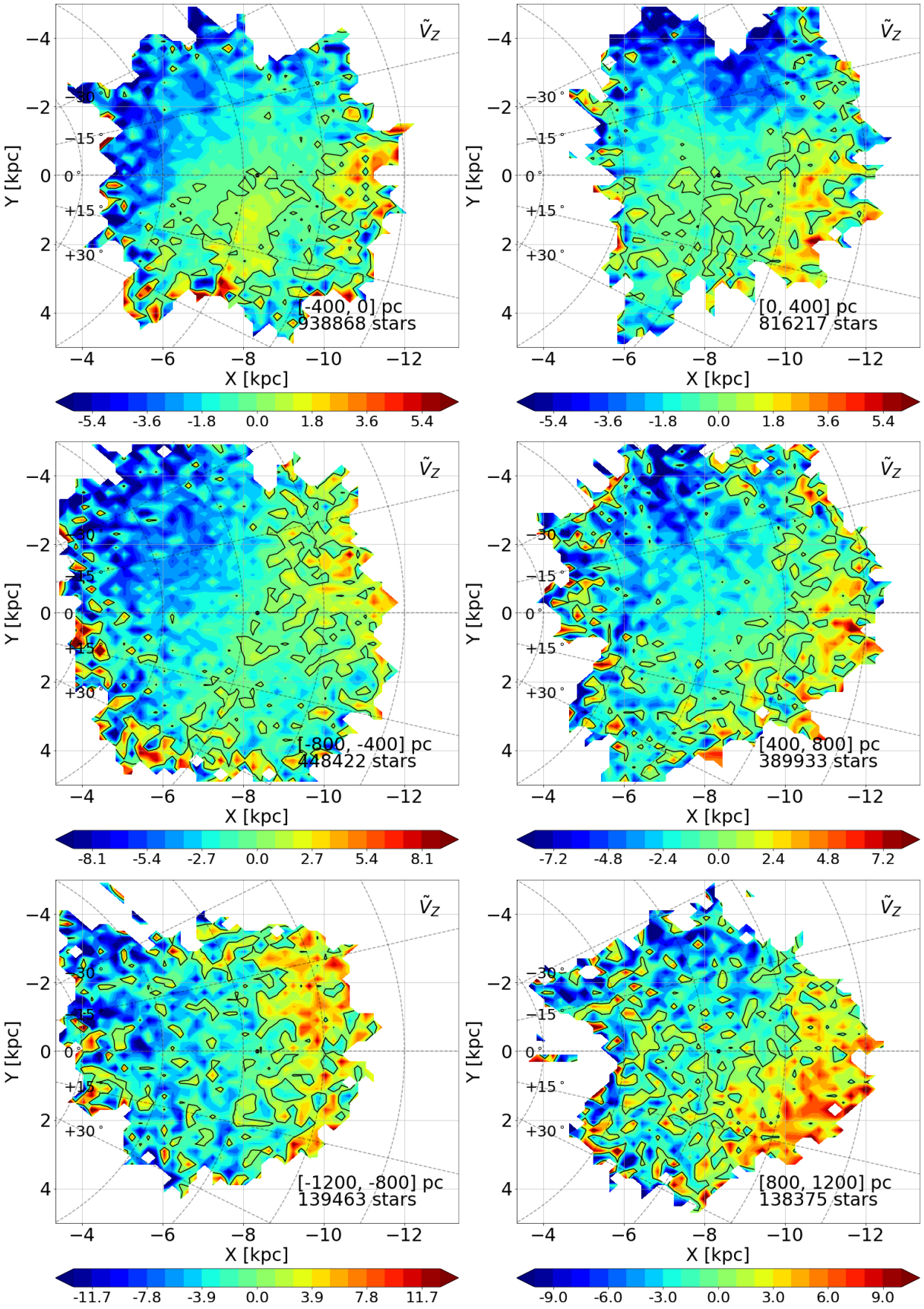

Fig. C.5. Same as Fig. C.1 for the median vertical velocity, $\tilde{V}_Z$. Here the disc has been divided into six layers. The southern Galactic hemisphere is on *left* and the northern is on the *right*. The distance to the Galactic mid-plane increases from *top* to *bottom*.

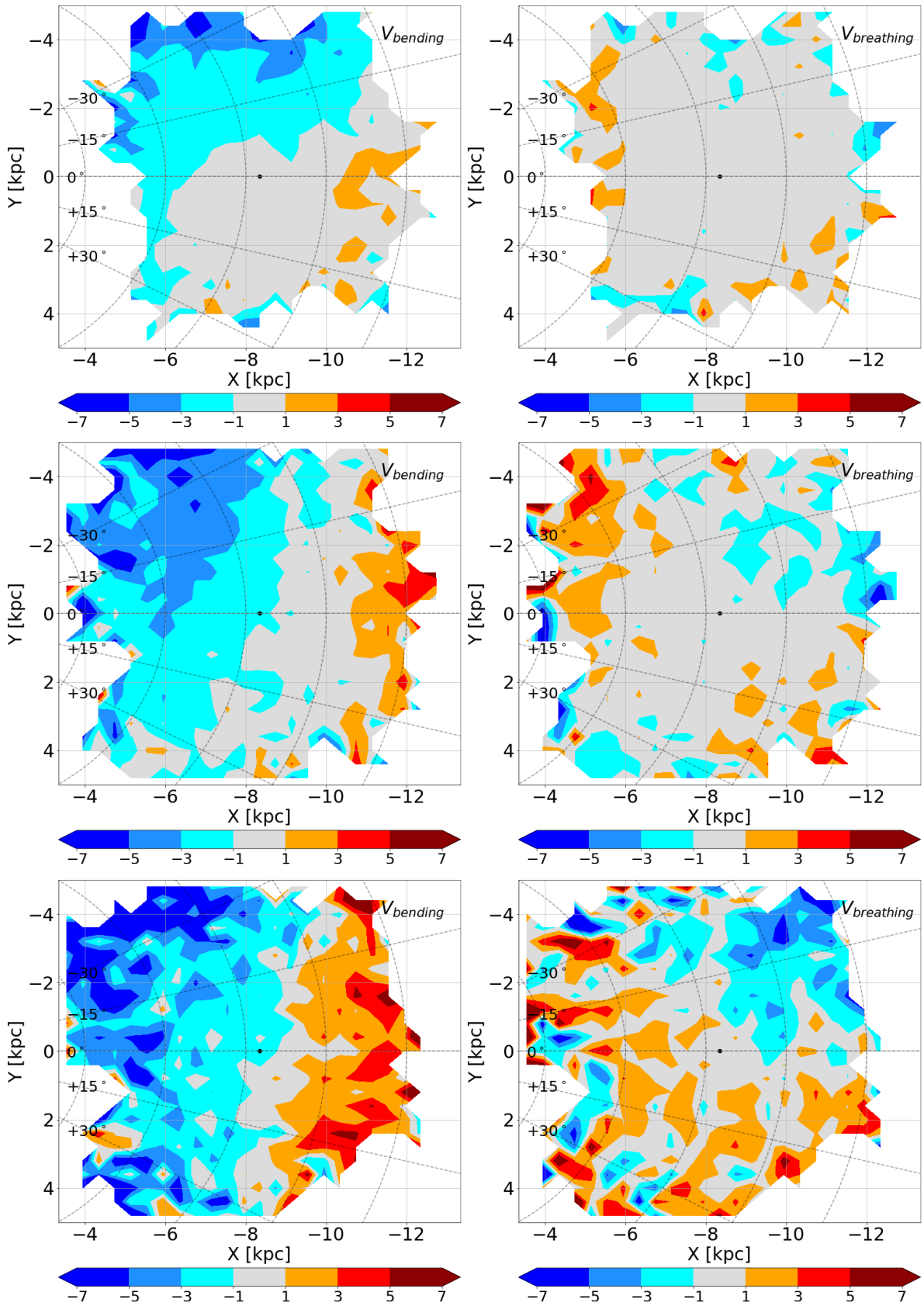

Fig. C.6. Same as Fig. C.1 for the bending (*left*) and breathing (*right*) velocities. Here the disc has been divided into three groups of symmetric layers. The distance to the Galactic mid-plane increases from *top* to *bottom*: $[-400, 0]$ and $[0, 400]$ pc (*top*), $[-800, -400]$ and $[400, 800]$ pc (*middle*), $[-1200, -800]$ and $[800, 1200]$ pc (*bottom*). The bending and breathing velocities have been calculated using larger (X, Y) cells than in the other maps of this appendix, i.e. 400 pc by 400 pc instead of 200 pc by 200 pc.

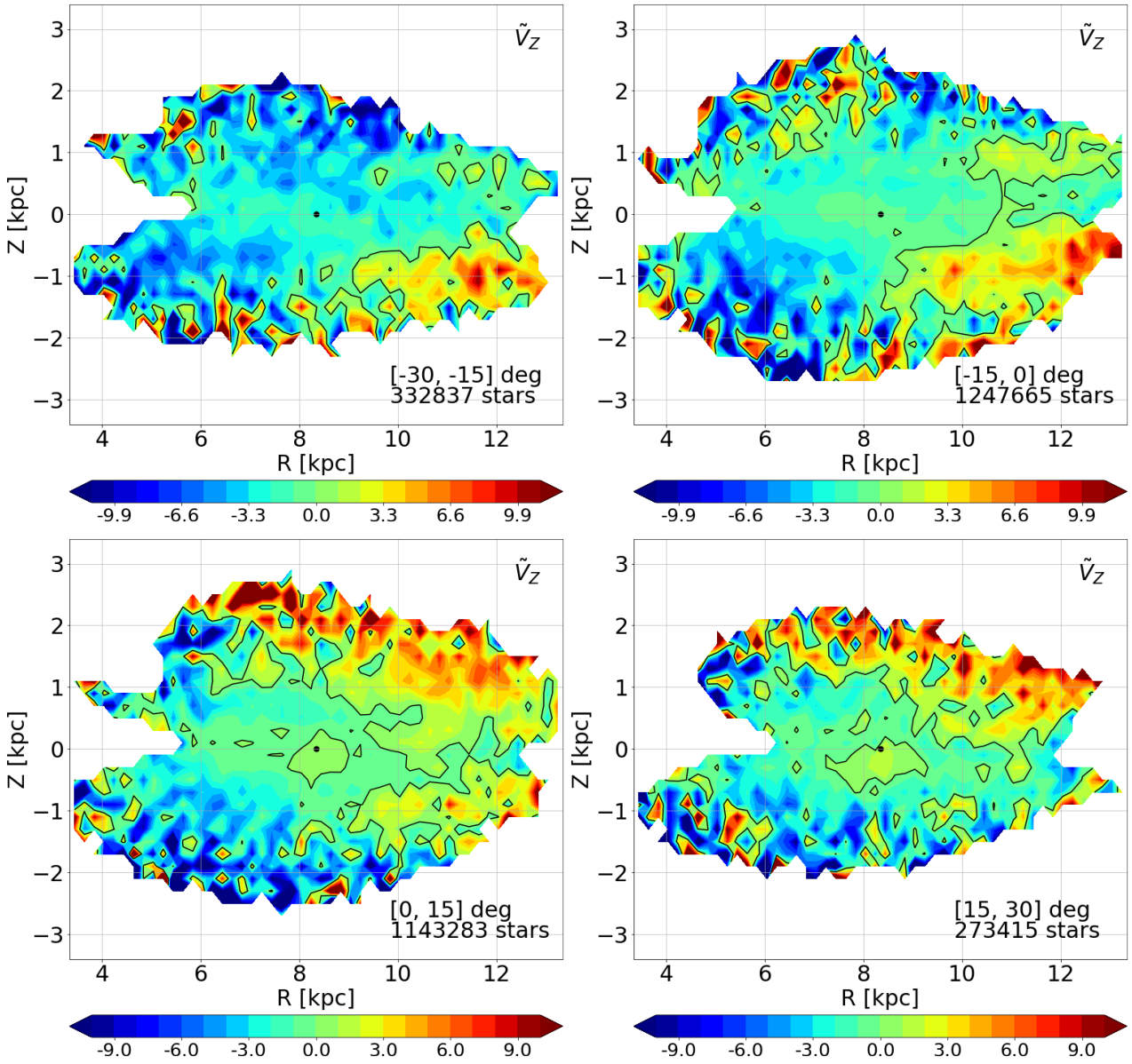

Fig. C.7. Same as Fig. C.2 for the median vertical velocity, $\tilde{V}_Z$.

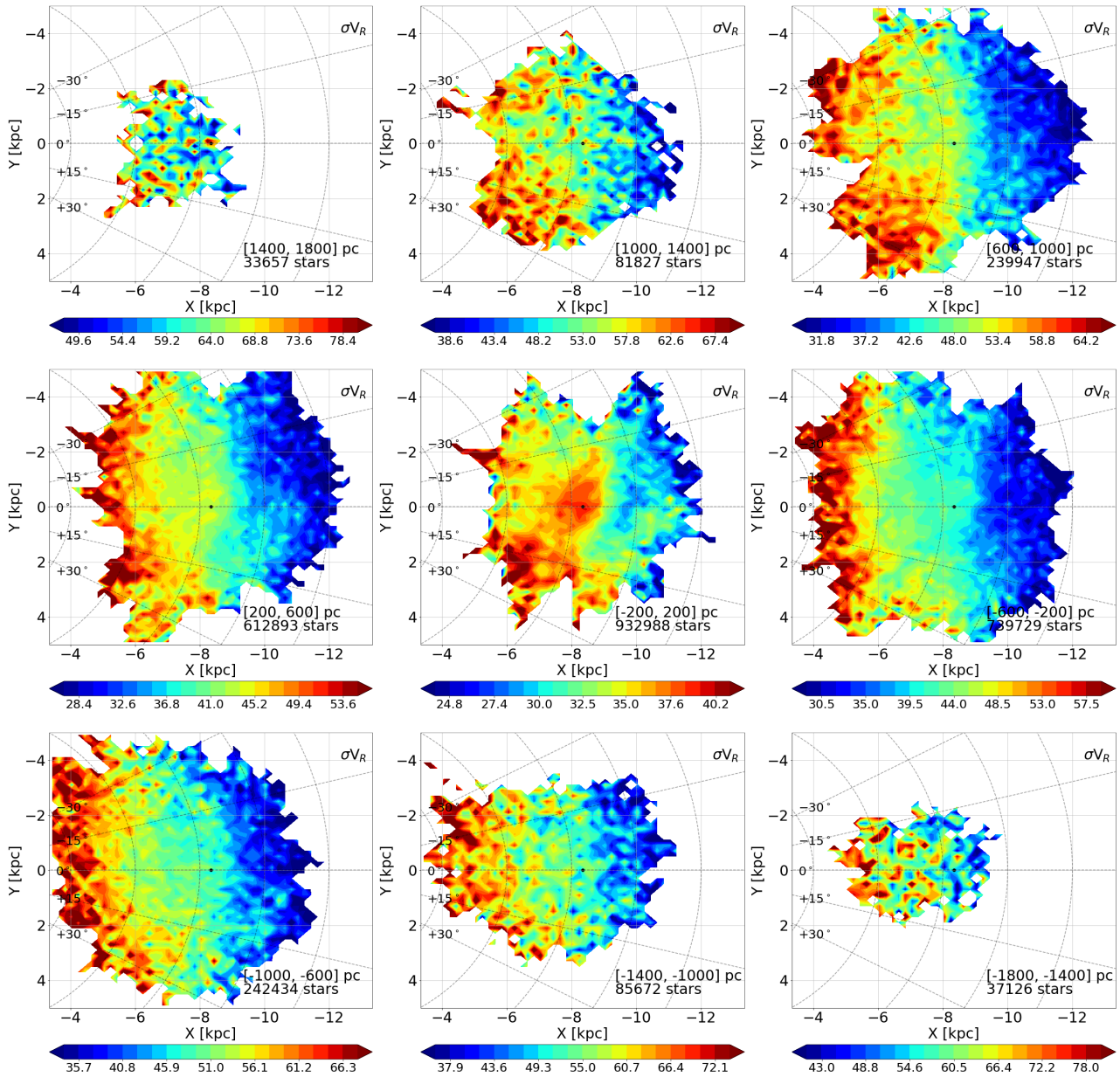

Fig. C.8. Same as Fig. C.1 for the radial velocity dispersion, σ_{V_R}.

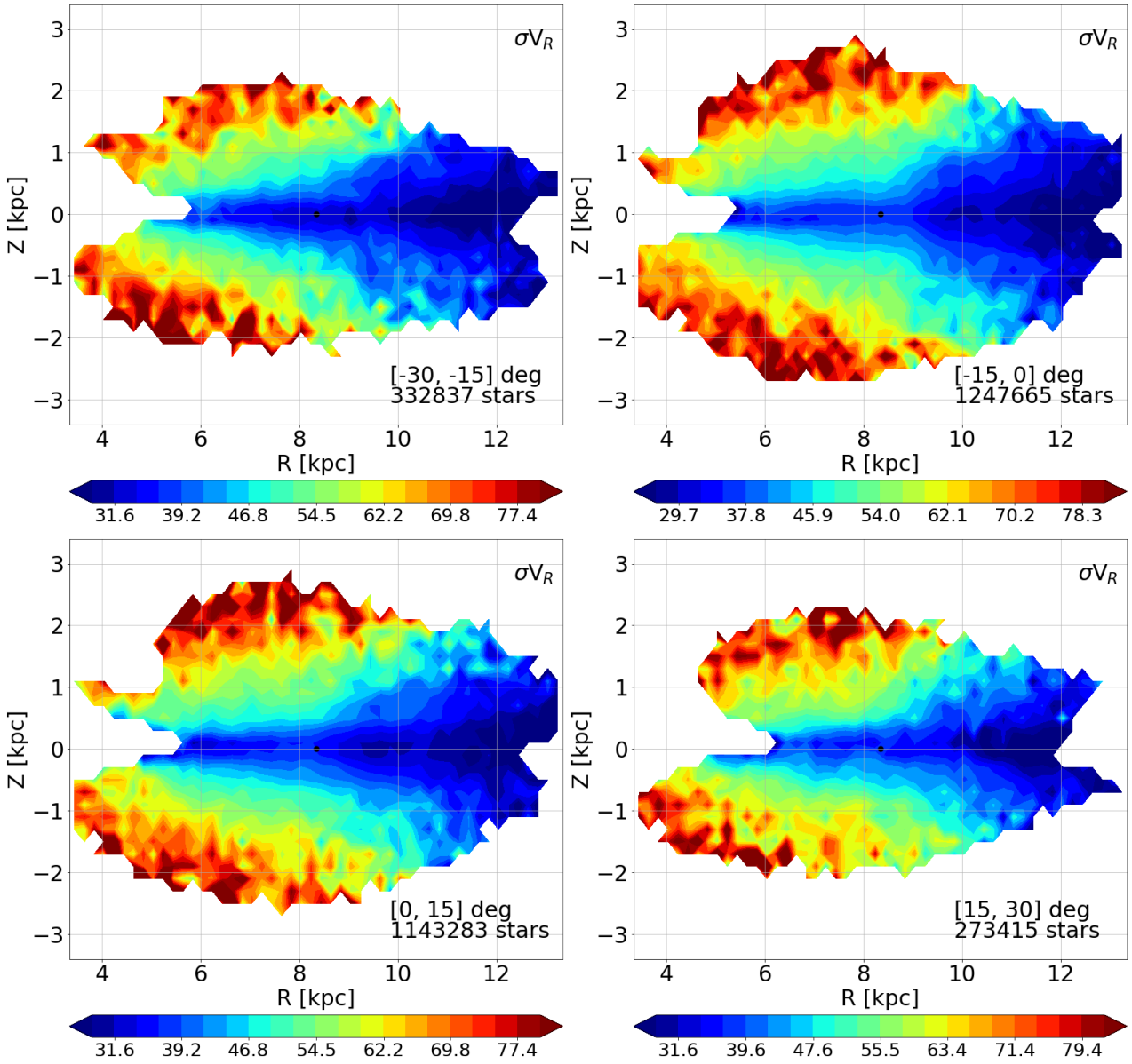

Fig. C.9. Same as Fig. C.2 for the radial velocity dispersion, σ_{V_R}.